Article

Carbon drawdown by algal blooms during Antarctic Cold Reversal from sedimentary ancient DNA

🔴 Check for updates

Josefine Friederike Weiß ®[1] ✉, Ulrike Herzschuh ®[1,2,3,9] ✉, Juliane Müller ®[4,5,6], Jie Liang[1], Maria-Elena Vorrath ®[7], Amedea Perfumo[1,8] & Kathleen R. Stoof-Leichsenring ®[1,9] ✉

The Southern Ocean plays a crucial role in the global carbon budget. One key interval for understanding this role is the Antarctic Cold Reversal (14,700–12,700 calibrated (cal) yr BP)—a Southern Hemisphere-specific cooling event that temporarily reversed the deglacial trend of warming and rising atmospheric CO_2. Modelling studies propose that the atmospheric CO_2 plateau during the Antarctic Cold Reversal is related to increased marine productivity. However, proxy constraints on the primary producer community are limited to the subset of groups that leave a fossil record. Here we applied ancient DNA shotgun metagenomics to samples from a marine sediment core to characterize the composition of the marine ecosystem across all trophic levels, finding that the haptophyte algae *Phaeocystis antarctica* was the dominant primary producer during the event. Independent proxy evidence from the same record points to high productivity in response to enhanced sea-ice seasonality caused by the cooling. Post Antarctic Cold Reversal, abrupt *Phaeocystis* community loss shows how sensitive this ecosystem is to warming, potentially representing a key tipping element. As an analogy for present warming, it highlights the importance of regions with high seasonal sea-ice variability and *Phaeocystis* dominance, such as the Ross Sea, in stabilizing atmospheric CO_2 content.

The Southern Ocean, surrounding the Antarctic continent, plays a key role in the global carbon budget[1]. It has been estimated to absorb more than 40% of the total anthropogenic CO_2 emissions since the industrialization[2]. Marine phytoplankton is the most important primary producer in the ocean and accounts for a large portion of CO_2 drawdown[3]. CO_2 assimilated by phytoplankton is exported in the form of organic carbon to deeper water layers (drawdown) and partly sequestered to the sediments (export). This so-called biological carbon pump operates as an important long-term carbon sink[4]. It is not yet understood how strongly global warming will impact the effectiveness of the biological carbon pump in the Southern Ocean[5], especially with the loss of sea ice[6].

The global warming at the end of the last glacial period (21,000–11,700 calibrated (cal) yr BP) was interrupted by a short cold period in the Southern Hemisphere, termed the Antarctic Cold Reversal (ACR; 14,700–12,700 cal yr BP)[7]. A previous study has shown that the sea-ice extent varied strongly between the seasons during the ACR[8]. It has been speculated, based on modelling, that the resulting high productivity and reduced outgassing facilitated a global CO_2 plateau and thus initiated a dampening feedback loop on global temperature during the ACR[8]. However, the palaeo-evidence is uncertain, mainly because we lack detailed proxy knowledge about past carbon drawdown and export during the ACR that may have led to a plateau in atmospheric

CO_2 concentrations[9]. Biogenic opal concentration in sediments is the most commonly used palaeoproductivity and carbon export proxy[10]. Studies have found a declining or stable low concentration of biogenic opal during the ACR[11], which is inconsistent with the assumption that diatom blooms in the Southern Ocean were of critical importance during the ACR CO_2 plateau[8]. High Ba/Fe ratios may indicate organic carbon drawdown in the Southern Ocean[12] as barite ($BaSO_4$) can precipitate during phytoplankton blooms[13], but records covering the ACR are lacking.

The composition of the primary producer community plays a major role in the speed and effectiveness of carbon drawdown and export because the productivity rates of the taxa differ[14]. Sea-ice conditions, in turn, determine the composition of the phytoplankton community[15] in the Southern Ocean[16]. Therefore, time series that place phytoplankton compositional turnover in the context of changing carbon drawdown and export, sea-ice conditions and atmospheric CO_2 are urgently needed.

The Antarctic Peninsula is known to be the fastest warming region of the Antarctic continent[17]. Nowadays, the marine ecosystem in this region is mainly influenced by open ocean conditions[3]. The primary producer community consists mainly of taxa associated with the open ocean[18], such as centric diatoms (for example, *Chaetoceros*)[19] and their primary consumer Antarctic krill[20], which is the main food source for top predators like whales and penguins[21].

In the past two decades, sedimentary ancient DNA (sedaDNA), a promising new palaeoecological proxy, has been established. This cutting-edge method, which analyses fragmented DNA strands bound to mineral particles in terrestrial and marine sedpiments, enables the characterization of biological community changes through time independently of fossil remains[22]. The sedaDNA metagenomic method is a non-target approach that bypasses the biases introduced by polymerase chain reaction (PCR) amplification[23], known from metabarcoding[24]. It allows the study of past communities at ecosystem level because it facilitates the detection of flora, fauna and microorganisms concurrently[25,26].

For this study, we examined a sediment core from the northern Antarctic Peninsula region, specifically the Bransfield Strait (PS97/072-1; Fig. 1), spanning the past 14,000 years. Using sedaDNA shotgun metagenomics, we identified *Phaeocystis antarctica* as the dominant primary producer during the ACR. We were able to detect the increase in carbon drawdown linked to elevated *P. antarctica* abundance during the ACR. Our findings reveal that as warming and a decrease in sea ice occurred, the modern ecosystem gradually established with the dominance of *Chaetoceros* at the beginning of the Holocene.

Phaeocystis dominated the phytoplankton community during the ACR

A total of 2,242,941 reads, retrieved from shotgun sequencing, were assigned to eukaryotic organisms including taxa from most of the major marine phyla (Supplementary Data 1 and 2). Our dataset is among the first marine datasets to allow an ecosystem-level reconstruction and is unique for the Southern Ocean in having high resolution covering the ACR and the transition to the Holocene.

Phytoplankton reads dominate the dataset (1,952,627; 87%). The haptophyte *P. antarctica* dominates the photoautotrophic community during the ACR, comprising over 60%. It is accompanied by pennate diatoms of the genus *Fragilariopsis* (for example, *Fragilariopsis cylindrus*), accounting for more than ~15% of the total community (Fig. 2). Additionally, we identify Chlorophyta such as *Micromonas* as primary producers at the end of the ACR with a relative abundance of approximately 10%. By analogy with present-day conditions, this primary producer community is associated with ecosystems that have a high sea-ice extent[15], such as the modern Ross Sea[27].

The ACR was a period of strong cooling in the Southern Hemisphere during deglacial warming, which is reflected in the European Project for

Ice Coring in Antarctica (EPICA) Dome C ice core[28]. Biomarker-based sea-ice reconstruction, the higher occurrence of sea-ice diatoms in the fossil record of core PS97/072-1 (ref. 11), and the estimated winter–summer sea-ice difference based on model results (Fig. 1) confirm a spatial and seasonal increase in sea-ice cover during the ACR (Fig. 2)[8].

The main pattern in the photoautotrophic community in this study is a shift in dominance from a haptophyte- to a diatom-dominated community (Fig. 2) approximately 12,700 cal yr BP at the end of the ACR (Supplementary Fig. 1). Throughout the Holocene, the community is dominated by *Chaetoceros* species. The shift seen in the palaeogenetic record at the end of the ACR is consistent with independent quantitative data on diatom concentration and biogenic opal (Supplementary Fig. 2 and Supplementary Table 1). Furthermore, qualitative changes in the composition can be seen in the independent morphological count data, which correlate significantly with the diatom data of the palaeogenetic record (Supplementary Table 1). Additionally, this shift is supported by a study from the Scotia Sea showing an increased abundance of Chaetocerotaceae since 12,700 cal yr BP[25].

Carbon drawdown associated with *Phaeocystis* during the ACR

We have substantial palaeo-evidence that the reconstructed *Phaeocystis*-dominated sea-ice community in the Southern Ocean during the ACR was accompanied by high carbon drawdown. Recent *Phaeocystis*-dominated communities are characterized by biomass-rich blooming owing to their strategy of forming colonies to reduce zooplankton grazing pressure[29,30]. Moreover, *P. antarctica* has significantly higher CO_2 absorption and export compared with diatoms and can achieve a near-maximum photosynthetic rate at low irradiances such as under sea ice[9,16].

Intensive phytoplankton blooming during the ACR is accompanied by the bacterioplankton signal in our core. We observe that the period of high *Phaeocystis* abundance has a high co-occurrence of methylotrophic bacteria specialized in single carbon compound metabolism in our prokaryote record[31]. From this we suggest that indications of methylotrophic bacteria may be used after further testing as a new palaeo-proxy for past algal blooms.

The Ba/Fe ratio is a well-established proxy for carbon drawdown and export productivity[12]. From element scanning of our sediment core, we observe a high Ba/Fe ratio during the *Phaeocystis*-rich ACR (Fig. 2 and Supplementary Data 3), suggesting increased productivity and drawdown of CO_2 within the water column. In contrast to Ba/Fe, total organic carbon values from the same core do not show a corresponding increase during the ACR[11] (Supplementary Fig. 3). This probably reflects differences in proxy preservation rather than a lack of carbon drawdown[13,32,33]. Additionally, the short duration of the ACR and subsequent warming probably intensified upwelling, promoting CO_2 outgassing from deeper water masses[34,35]. However, our study does not aim to quantify long-term carbon burial in the sediment, as this is not the primary focus. Instead, our results emphasize increased carbon drawdown during the ACR.

We applied a piecewise structural equation model (SEM) to analyse temporal correlations between palaeogenetic data and environmental parameters (Fig. 3a). This allowed us to test our hypothesis that *Phaeocystis* plays a substantial role in the carbon cycle during the ACR[36]. The results, indicated by the favourable goodness-of-fit statistics (P value = 0.87 for Fisher's C and P value = 0.331 for chi-squared statistics) and the low Akaike information criterion (AIC) value (791,856), demonstrate that this model is the most appropriate for estimating the relationships between the factors (Supplementary Data 4). The SEM revealed a significant influence of temperature (from EDC δD‰, the EPICA Dome C deuterium record) and sea ice (index derived from phytoplankton-derived IP_{25} biomarker for the Southern Ocean: $PIPSO_{25}$), on the abundance of specific phytoplankton groups as reflected by standardized path coefficients (β) (*Phaeocystis* ($\beta = -0.33$;
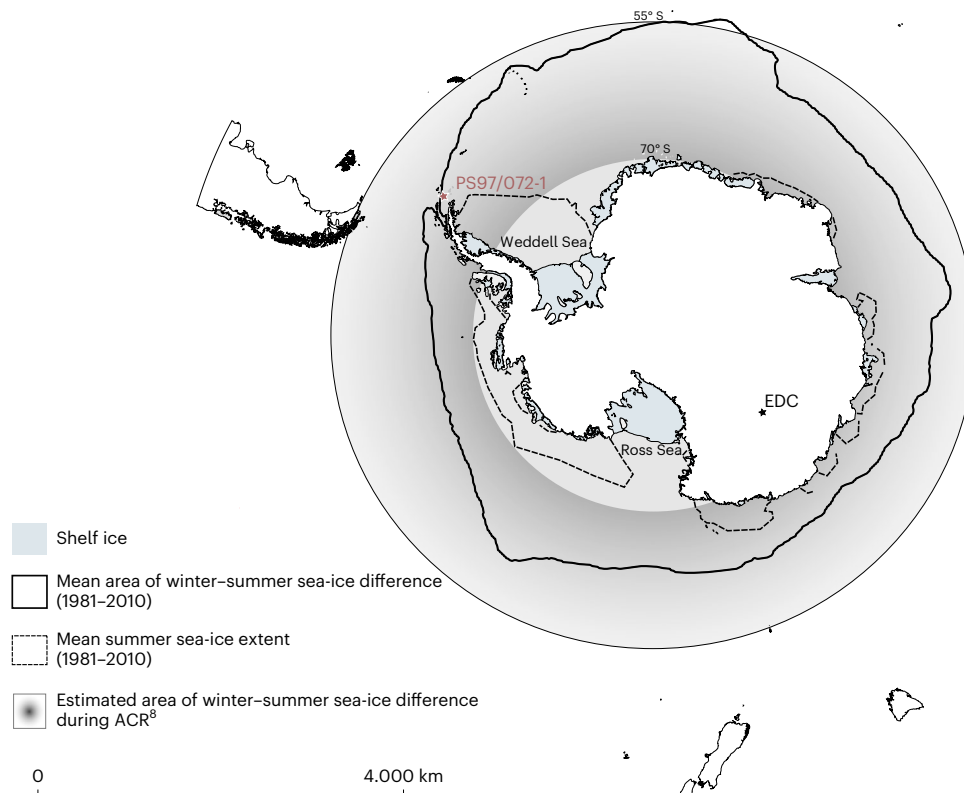
Fig. 1 | Seasonal difference in sea-ice area over the ACR and the past 20 years around Antarctica, showing the locations of marine sediment core PS97/072-1 and ice core EPICA Dome C. The mean area (approximately 15 million km²) between 1981 and 2010 of winter–summer sea-ice difference is shown in light grey[56]. The modelled difference between winter sea-ice area (sea-ice extent up to 55° S in winter) and summer sea-ice area (sea-ice extent up to 70° S) during the ACR is shown as a gradient grey area and reaches up to 20 million km² (ref. [8]). EDC, EPICA Dome C. Basemap created with the SCAR Antarctic Digital Database version 7.0 (ref. [57]), part of Quantarctica 3.2 (ref. [58]).

$\beta = 0.59$), *Fragilariopsis* (sea-ice diatoms; $\beta = -0.48$; $\beta = 0.49$) and *Chaetoceros* (open-water diatoms; $\beta = 0.56$; $\beta = -0.43$)) during the ACR (Fig. 3a). Notably, *Phaeocystis* abundance was significantly negatively associated with atmospheric CO_2 concentrations ($\beta = -0.52$) and significantly positively associated with the carbon drawdown proxy (Ba/Fe ratio, $\beta = 0.74$; Fig. 3a). These standardized path coefficients indicate that an increase in *Phaeocystis* abundance was linked to enhanced CO_2 drawdown, suggesting its important role in the carbon cycle during the ACR. Additionally, *Phaeocystis* and methylotrophic bacteria exhibited significantly temporally coherent changes synchronized abundance fluctuations ($\beta = 0.38$), further supporting the hypothesis of a relationship between *Phaeocystis* blooms and carbon drawdown. In contrast, neither *Fragilariopsis* nor *Chaetoceros* showed significant positive relationships with carbon drawdown, highlighting the distinctive role of *Phaeocystis* in this process (Fig. 3a).

To assess the possible contribution of dominant phytoplankton groups to carbon drawdown, we used literature-derived net primary production (NPP) values for *P. antarctica* and other key primary producers such as *Fragilariopsis* and *Chaetoceros*. In the Ross Sea, *P. antarctica* showed an average NPP (mean ± s.d.) of 77.5 ± 47.2 gC m^{-2} yr^{-1}, while sea-ice diatoms like *Fragilariopsis* reach an average NPP of 38.9 ± 12.1 gC m^{-2} yr^{-1} (ref. [37]). In contrast, the diatom-dominated modern Western Antarctic Peninsula had a lower NPP of 15.83 ± 5.24 gC m^{-2} yr^{-1} (ref. [38]). These values were provided with uncertainty ranges accounting for environmental and ecological factors, which we also used to calculate carbon drawdown. Using these NPP values and sea-ice extent data, we estimated a possible range of CO_2 drawdown over the 1,800 years of the ACR (Fig. 3b). Primary production of *Phaeocystis* could have led to an atmospheric CO_2 drawdown of up to 20.64 ± 7.30 ppmv CO_2, while *Fragilariopsis* and Western Antarctic Peninsula diatoms

(for example, *Chaetoceros*) could accumulate 10.36 ± 4.14 ppmv and 4.23 ± 1.7 ppmv, respectively. Pre-ACR, the total accumulated CO_2 of *P. antarctica* was estimated at 69.19 ± 27.68 ppmv, while for sea-ice diatoms like *Fragilariopsis*, it would have been 34.73 ± 13.89 ppmv. For the timeframes (pre-ACR, ACR and post-ACR), we selected the model variant that yielded the smallest mean difference from the actual CO_2 concentrations, as this variant most accurately reflected the observed CO_2 progression during the ACR (Supplementary Fig. 4).

Our CO_2 drawdown calculation (Fig. 3b) suggests that the shift from diatom to *Phaeocystis* dominance with the onset of the ACR may best explain the actual CO_2 trends of the past. A paired *t*-test confirmed no significant difference between the CO_2 captured by *Phaeocystis* and the actual or modelled CO_2 progression during the ACR (P value = 0.85, mean difference = −0.11; Supplementary Fig. 4). Previous studies have documented higher biogenic opal values during the pre-ACR period (Supplementary Fig. 2)[8,39] and high counts of *Chaetoceros* resting spores at that time[40,41], indicating a dominance of open-water-associated diatoms before the ACR. Our CO_2 drawdown calculation (Fig. 3b) supports these findings, showing no significant difference between the CO_2 captured by *Chaetoceros* and the actual CO_2 curve during the pre-ACR period (P value = 0.27, mean difference = 0.32). While our dataset provides insights into community composition during and after the ACR, the lack of sedaDNA samples from earlier periods limits our understanding of pre-ACR community composition, highlighting the need for future studies targeting older sedimentary records. The projection of the NPP of *Chaetoceros* or *Fragilariopsis* was rejected. Overall, our results highlight the potential importance of *Phaeocystis* blooms in enhancing CO_2 drawdown during the ACR.

While a comprehensive model would require incorporating ocean circulation, carbon cycling and CO_2 exchange across the
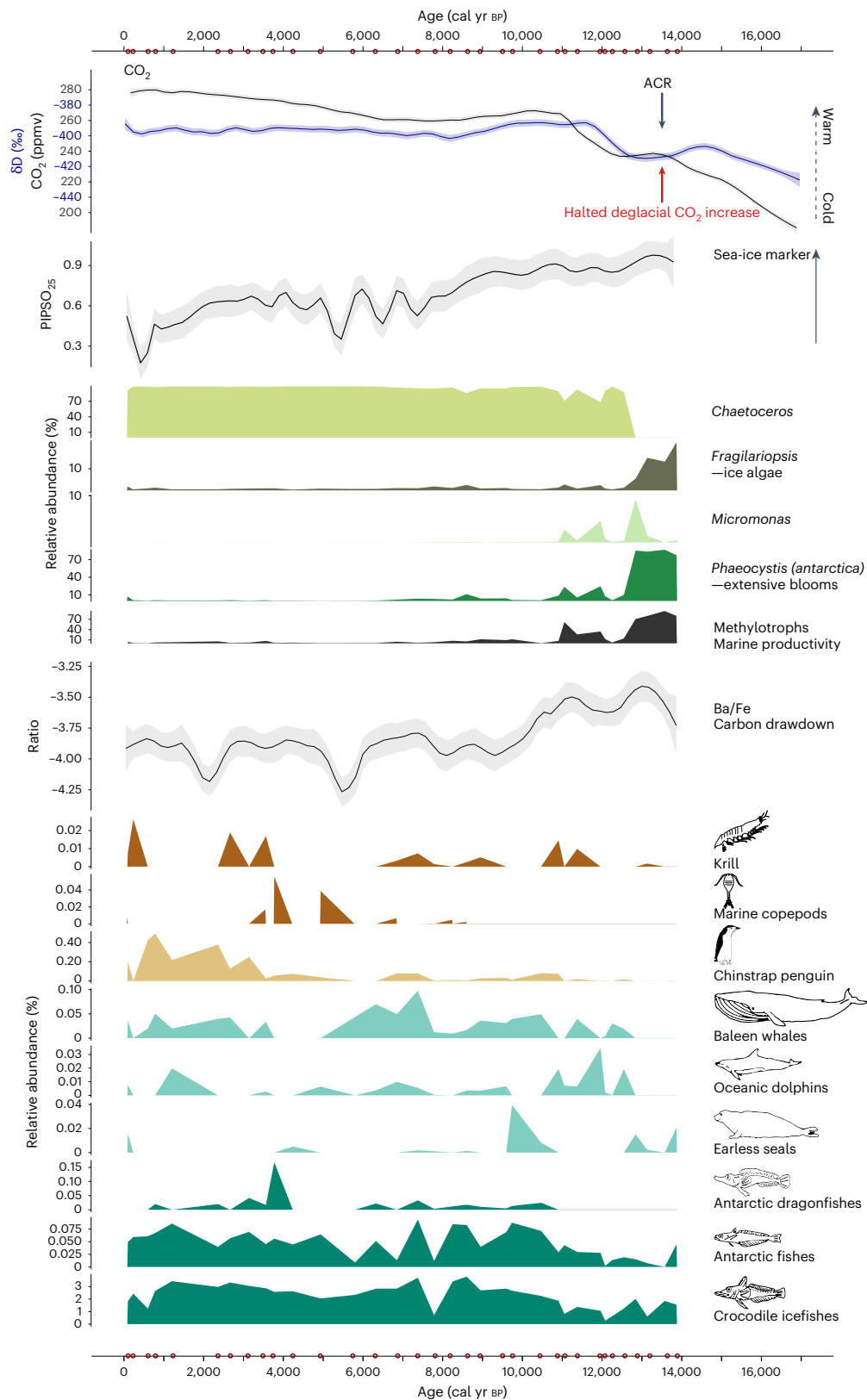
Fig. 2 | Primary producers and higher trophic level community composition over time. The uppermost graph shows the δD‰ (ref. [28]) values for temperature reconstructions and the reconstructed atmospheric CO_2 concentrations of the EPICA Dome C ice core for the past 17,000 years[59]. The dark grey arrow indicates the ACR and the red arrow marks the halted deglacial CO_2 rise. Below that is the $PIPSO_{25}$ sea-ice biomarker graph over the past 14,000 years derived from the PS97/72-01 core[11]. Next are the dominant primary producer taxa derived from shotgun metagenomics of sedaDNA over the past 14,000 years. In addition, the relative abundance of methylotrophic bacteria is shown, as well as the Ba/Fe ratio derived from elemental scanning. Shaded areas in all panels indicate 95% confidence intervals reflecting the uncertainty of the measurements or reconstructions. Finally, reconstructed ecosystem community composition of higher trophic levels including only Antarctic taxa over the past 14,000 years. The red dots on the x axis show the discrete sampling points for sedaDNA shotgun metagenomics.
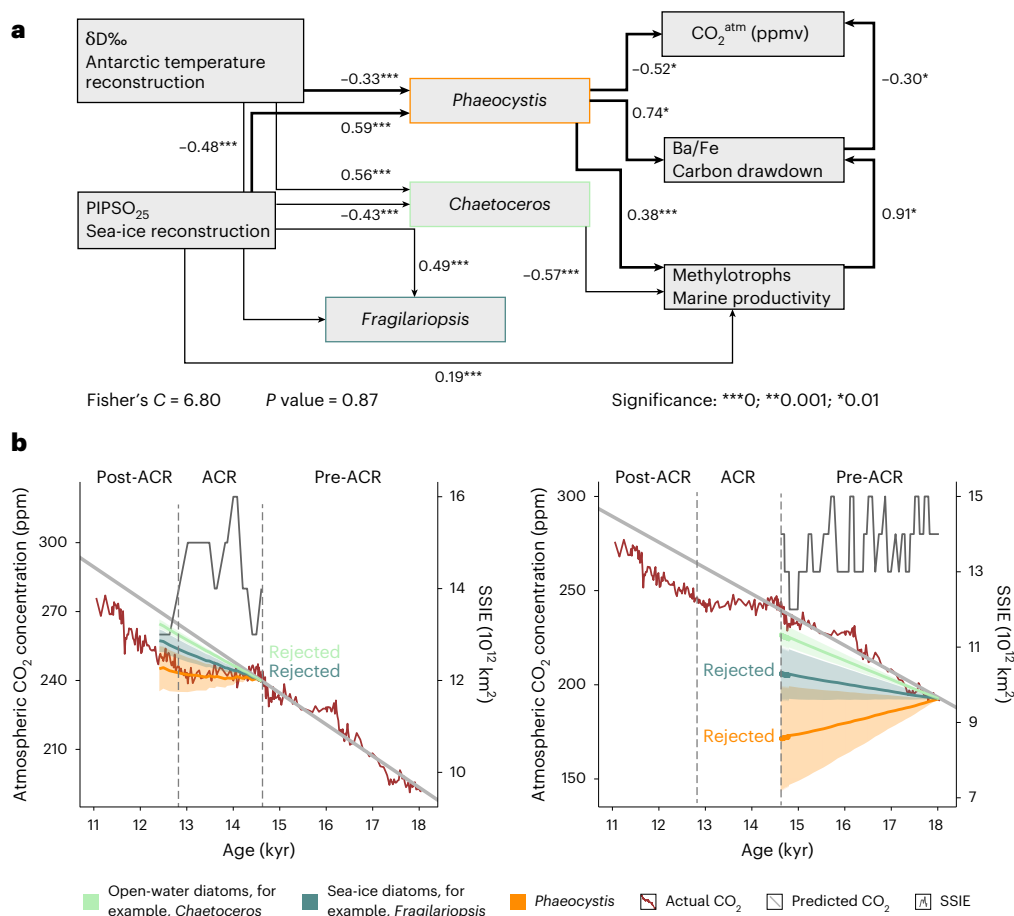
Fig. 3 | Relationships between environmental variables and paleogenetic data of primary producers, and their modeled impact on atmospheric CO₂ across time. a, The piecewise structural equation model (SEM) illustrates the relationship between environmental parameters as temperature and sea ice, and paleogenetic data of major primary producers over time. Arrow direction indicates assumed causality; standardized path coefficients (β) denote the strength and direction (positive/negative) of effects. Significance is marked by asterisks (see legend). Model fit: Fisher's $C = 6.80$, $P = 0.87$. **b**, Seasonal sea-ice

extent (SSIE; 10^{12} km²) and modelled impact of average NPP of different primary producers, combined with varying flux efficiencies (30%, 50%, 70%) from the atmosphere to surface waters, on global atmospheric carbon dioxide (CO_2^{atm}) concentrations (ppmv) before, during and after the ACR. Left panel: cumulative NPP impact during and after the ACR; right panel: before the ACR. Data are shown as medians with shading indicating median ± standard deviation. Hypotheses attributing carbon drawdown to any single taxon (colour-coded as 'rejected') were tested via two-sided paired t-tests with no correction for multiple testing required.

ocean–atmosphere interface, our study emphasizes the substantial biological contributions to CO_2 drawdown. To assess the role of locally dominating primary producers, we projected CO_2 drawdown using a pre-industrial partial pressure of CO_2 (pCO_2) baseline, varying fluxes between the atmosphere and ocean, different NPP values, and seasonal sea-ice extent as the primary production area. While our simplified model captures key CO_2 trends during the ACR, uncertainties remain due to assumptions regarding NPP values derived from modern analogues, the spatial extrapolation and the absence of sedaDNA samples pre-dating the ACR. However, our approach reproduces the observed variation in atmospheric CO_2 changes, suggesting that biological processes, particularly shifts in primary producers, played a contributing role in shaping atmospheric CO_2 levels during the ACR.

By utilizing palaeo-proxies, statistical modelling and projection to assess the influence of NPP values of different primary producers on global CO_2 concentrations during the ACR, our findings strongly indicate that *P. antarctica*, as the dominant species, played an important role in the heightened CO_2 removal and potential carbon export. This aligns with studies of the modern Southern Ocean ecosystem indicating that carbon drawdown of *P. antarctica* is more rapid and efficient compared with other groups of phytoplankton[9,16].

Shifts in phytoplankton composition may also affect the global sulfur cycle, as *Phaeocystis* produces more dimethyl sulfide than

diatoms[42]. Therefore, we also hypothesize positive feedback of *Phaeocystis* dominance on climate through its influence on cloud formation with higher dimethyl sulfide production[43]. With a disappearance of *Phaeocystis* in the high-latitude regions, dimethyl sulfide production would decrease by 7.7%, which in turn would lead to fewer clouds and thus to a warmer climate[44].

Ecosystem shift at the onset of warming after the ACR

Our sedaDNA record allows insights into the past Antarctic ecosystem covering the ACR and the Holocene. For example, characteristic Antarctic ice fish families (Notothenioidei) and penguin taxa were detected in a sedaDNA palaeorecord. Relatively irregular signals of taxa from higher trophic levels may depend on the low biomass of consumers (approximately 30%, mainly arthropods and fishes) compared with primary producers (approximately 70%)[45,46]. The ACR showed a distinct ecosystem with Channichthyidae (crocodile ice fish) as the dominant taxa, along with indications of the Phocidae (earless seals) family, while *Pleuragramma* (Nototheniidae), a key prey ice fish species[47] in the modern Ross Sea, was abundant (Fig. 2). The ecosystem during the ACR resembled the modern Ross Sea shelf region with low zooplankton and top predator abundance, suggesting a less linear food web[48–50].
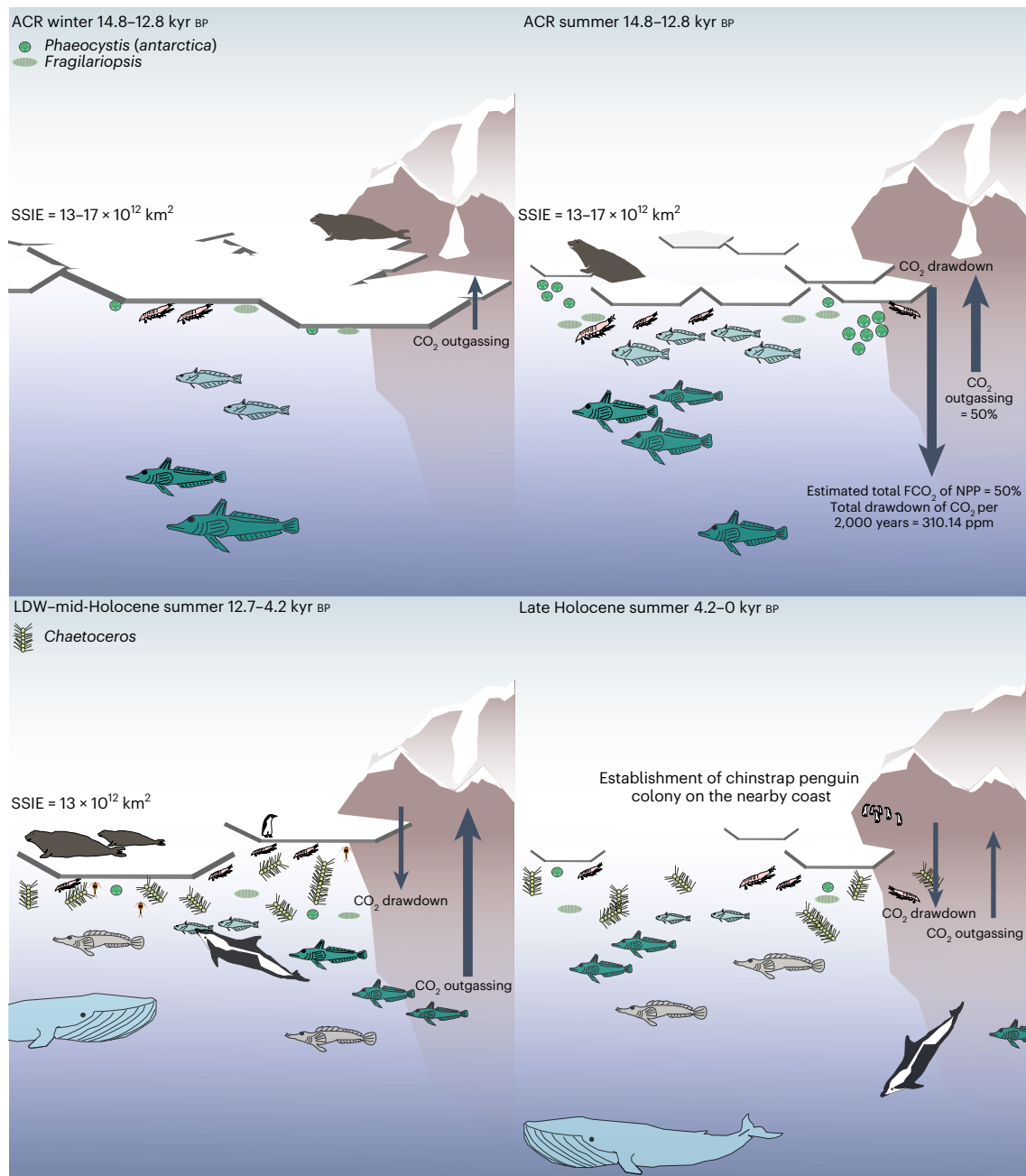
Fig. 4 | Seasonal and long-term ecosystem reconstructions of the Antarctic Cold Reversal (ACR) and post-ACR warming periods inferred from sedimentary ancient DNA shotgun metagenomics. Upper panel: seasonal ecosystem reconstruction of the ACR. The left side shows the reconstructed winter conditions in the Bransfield Strait with an indication of sea-ice coverage and glaciation of the nearby coast. The thickness of the dark grey arrow and its direction indicate the suspected strength of outgassing of CO_2 (ref. 8) defined as FCO_2 within the figure. On the right side the reconstructed ecosystem of the summer during the ACR is depicted. The dark grey arrow, depending on its direction, indicates either the strength of outgassing or the strength of carbon drawdown. Lower panel: summer ecosystem reconstruction of the late deglacial warming (LDW) until the mid-Holocene and mid-Holocene until the late Holocene. The left side shows the speculated ecosystem of the Bransfield Strait during the LDW, early Holocene and mid-Holocene. The dark grey arrow, depending on its direction, indicates either the strength of outgassing or the strength of carbon drawdown. On the right side, the ecosystem community reconstructed for the late Holocene is shown.

With the onset of Holocene warming, Nototheniidae, the cetacean family Balaenopteridae (rorquals) and Delphinidae (dolphins) increased in abundance, while *Pygoscelis antarcticus* (chinstrap penguin) expanded only in the late Holocene (Fig. 4). It is known that the main prey of chinstrap penguins, Antarctic krill, prefers diatoms over *Phaeocystis*[51,52]. Additionally, the establishment of the penguin population in the Antarctic Peninsula region occurred during the late Holocene and was probably favoured by ice-free nesting sites[53] and reduced sea-ice cover[11]. The limited preservation of macro-zooplankton and

benthic taxa in sedaDNA studies could be attributed to grazing and database limitations, respectively[54].

Implications and conclusion
With our study we show that sedaDNA enables the reconstruction of past Antarctic communities with high completeness and taxonomic resolution. This study shows that productivity proxies, which exclude major photoautotrophic groups like *Phaeocystis*, are only of limited use.

We identified major *Phaeocystis* blooming events and related increased carbon drawdown during the ACR to an atmospheric CO_2 plateau (Figs. 2 and 3). This provides the hitherto missing piece of evidence to identify past Antarctic phytoplankton productivity as a major negative feedback in the global carbon cycle during a period of global warming. As an analogy for ongoing warming, it highlights the importance of regions with high seasonal sea-ice variability and *Phaeocystis* dominance, such as the Ross Sea, to stabilize the atmospheric CO_2 content.

Based on our reasoning, we anticipate that simulations using models parameterized/validated with diatom productivity observations probably underestimate the Antarctic carbon pump function of sea-ice impacted regions[55]. However, our finding of a haptophyte-to-diatom turnover in the course of temperature increase shows how sensitive this ecosystem is to warming, potentially representing a key tipping element in the global carbon cycle (Fig. 4).

Online content

Any methods, additional references, Nature Portfolio reporting summaries, source data, extended data, supplementary information, acknowledgements, peer review information; details of author contributions and competing interests; and statements of data and code availability are available at https://doi.org/10.1038/s41561-025-01761-w.

References

1. Rintoul, S. R. The global influence of localized dynamics in the Southern Ocean. *Nature* **558**, 209–218 (2018).
2. Long, M. C. et al. Strong Southern Ocean carbon uptake evident in airborne observations. *Science* **374**, 1275–1280 (2021).
3. Arrigo, K. R., van Dijken, G. L., & Bushinsky, S. Primary production in the southern ocean, 1997–2006. *J. Geophys. Res. Oceans* https://doi.org/10.1029/2007JC004578 (2008).
4. Hauck, J. et al. On the Southern Ocean CO_2 uptake and the role of the biological carbon pump in the 21st century. *Glob. Biogeochem. Cycles* **29**, 1451–1470 (2015).
5. Hauck, J., Lenton, A., Langlais, C. & Matear, R. The fate of carbon and nutrients exported out of the Southern Ocean. *Glob. Biogeochem. Cycles* **32**, 1556–1573 (2018).
6. Moreau, S., Boyd, P. W. & Strutton, P. G. Remote assessment of the fate of phytoplankton in the Southern Ocean sea-ice zone. *Nat. Commun.* **11**, 3108 (2020).
7. EPICA community members. Eight glacial cycles from an Antarctic ice core. *Nature* **429**, 623–628 (2004).
8. Fogwill, C. J. et al. Southern Ocean carbon sink enhanced by sea-ice feedbacks at the Antarctic Cold Reversal. *Nat. Geosci.* **13**, 489–497 (2020).
9. DiTullio, G. R. et al. Rapid and early export of Phaeocystis antarctica blooms in the Ross Sea, Antarctica. *Nature* **404**, 595–598 (2000).
10. Kim, S. et al. Biogenic opal production changes during the mid-Pleistocene transition in the Bering Sea (IODP Expedition 323 Site U1343). *Quat. Res.* **81**, 151–157 (2014).
11. Vorrath, M. E. et al. Deglacial and Holocene sea-ice and climate dynamics in the Bransfield Strait, northern Antarctic Peninsula. *Clim. Past* **19**, 1061–1079 (2023).
12. Jaccard, S. L. et al. Two modes of change in Southern Ocean productivity over the past million years. *Science* **339**, 1419–1423 (2013).
13. Dymond, J., Suess, E. & Lyle, M. Barium in deep-sea sediment: a geochemical proxy for paleoproductivity. *Paleoceanography* **7**, 163–181 (1992).
14. Richardson, T. L. & Jackson, G. A. Small phytoplankton and carbon export from the surface ocean. *Science* **315**, 838–840 (2007).
15. Arrigo, K. R., Worthen, D. L., Lizotte, M. P., Dixon, P., & Dieckmann, G. Primary production in Antarctic sea ice. *Science* **276**, 394–397 (1997).
16. Arrigo, K. R. et al. Phytoplankton community structure and the drawdown of nutrients and CO_2 in the Southern Ocean. *Science* **283**, 365–367 (1999).
17. Vaughan, D. G. et al. Recent rapid regional climate warming on the Antarctic Peninsula. *Climatic Change* **60**, 243–274 (2003).
18. Schofield, O. et al. Decadal variability in coastal phytoplankton community composition in a changing West Antarctic Peninsula. *Deep Sea Res. I* **124**, 42–54 (2017).
19. Grigorov, I., Rigual-Hernandez, A. S., Honjo, S., Kemp, A. E. & Armand, L. K. Settling fluxes of diatoms to the interior of the Antarctic circumpolar current along 170 W. *Deep-Sea Res. I* **93**, 1–13 (2014).
20. Cleary, A. C., Durbin, E. G. & Casas, M. C. Feeding by Antarctic krill *Euphausia superba* in the West Antarctic Peninsula: differences between fjords and open waters. *Mar. Ecol. Prog. Ser.* **595**, 39–54 (2018).
21. Trathan, P. N. & Hill, S. L. The importance of krill predation in the Southern Ocean. *In Biology and Ecology of Antarctic Krill*. 321–350 (Springer, 2016).
22. Wang, K. et al. 4000-year-old hair from the Middle Nile highlights unusual ancient DNA degradation pattern and a potential source of early eastern Africa pastoralists. *Sci. Rep.* **12**, 20939 (2022).
23. Armbrecht, L. et al. Paleo-diatom composition from Santa Barbara Basin deep-sea sediments: a comparison of 18S-V9 and diat-rbcL metabarcoding vs shotgun metagenomics. *ISME Commun.* **1**, 66 (2021).
24. Zimmermann, H. H. et al. Sedimentary ancient DNA from the subarctic North Pacific: how sea ice, salinity, and insolation dynamics have shaped diatom composition and richness over the past 20,000 years. *Paleoceanogr. Paleoclimatol.* **36**, e2020PA004091 (2021).
25. Armbrecht, L. et al. Ancient marine sediment DNA reveals diatom transition in Antarctica. *Nat. Commun.* **13**, 5787 (2022).
26. Zimmermann, H. H. et al. Marine ecosystem shifts with deglacial sea-ice loss inferred from ancient DNA shotgun sequencing. *Nat. Commun.* **14**, 1650 (2023).
27. Rizkallah, M. R. et al. Deciphering patterns of adaptation and acclimation in the transcriptome of *Phaeocystis antarctica* to changing iron conditions. *J. Phycol.* **56**, 747–760 (2020).
28. Jouzel, J. et al. Orbital and millennial Antarctic climate variability over the past 800,000 years. *Science* **317**, 793–796 (2007).
29. Balaguer, J. et al. Iron and manganese availability drives primary production and carbon export in the Weddell Sea. *Curr. Biol.* **33**, 4405–4414 (2023).
30. Zhang, Y., Zhao, W., Wei, H., Yang, W. & Luo, X. Iron limitation and uneven grazing pressure on phytoplankton co-lead the seasonal species succession in the Ross Ice Shelf polynya. *J. Geophys. Res. Oceans* **128**, e2022JC019026 (2023).
31. Mincer, T. J. & Aicher, A. C. Methanol production by a broad phylogenetic array of marine phytoplankton. *PLOS One* **11**, e0150820 (2016).
32. Ma, Z. et al. Carbon sequestration during the Palaeocene–Eocene Thermal Maximum by an efficient biological pump. *Nat. Geosci.* **7**, 382–388 (2014).
33. Schoepfer, S. D. et al. Total organic carbon, organic phosphorus, and biogenic barium fluxes as proxies for paleomarine productivity. *Earth Sci. Rev.* **149**, 23–52 (2015).
34. Bauska, T. K. et al. Carbon isotopes characterize rapid changes in atmospheric carbon dioxide during the last deglaciation. *Proc. Natl Acad. Sci. USA* **113**, 3465–3470 (2016).
35. Sarmiento, J. L. et al. Trends and regional distributions of land and ocean carbon sinks. *Biogeosciences* **7**, 2351–2367 (2010).

36. Garcés-Pastor, S. et al. High resolution ancient sedimentary DNA shows that alpine plant diversity is associated with human land use and climate change. *Nat. Commun.* **13**, 6559 (2022).

37. Arrigo, K. R. & van Dijken, G. L. Interannual variation in air–sea CO_2 flux in the Ross Sea, Antarctica: a model analysis. *J. Geophys. Res. Oceans* **112**, (2007).

38. Kwon, Y. S., La, H. S., Kang, H. W. & Park, J. A regional-scale approach for modeling primary production and biogenic silica export in the Southern Ocean. *Environ. Res.* **217**, 114811 (2023).

39. Sikes, E. L. et al. Southern Ocean glacial conditions and their influence on deglacial events. *Nat. Rev. Earth Environ.* **4**, 454–470 (2023).

40. Bianchi, C. & Gersonde, R. Climate evolution at the last deglaciation: the role of the Southern Ocean. *Earth Planet. Sci. Lett.* **228**, 407–424 (2004).

41. Melis, R. et al. Last Glacial Maximum to Holocene paleoceanography of the northwestern Ross Sea inferred from sediment core geochemistry and micropaleontology at Hallett Ridge. *J. Micropalaeontol.* **40**, 15–35 (2021).

42. Wang, S., Elliott, S., Maltrud, M. & Cameron-Smith, P. Influence of explicit *Phaeocystis* parameterizations on the global distribution of marine dimethyl sulfide. *J. Geophys. Res. Biogeosci.* **120**, 2158–2177 (2015).

43. Stefels, J., Steinke, M., Turner, S., Malin, G. & Belviso, S. Environmental constraints on the production and removal of the climatically active gas dimethyl sulphide (DMS) and implications for ecosystem modelling. *Biogeochemistry* **83**, 245–275 (2007).

44. Wang, S., Maltrud, M. E., Burrows, S. M., Elliott, S. M. & Cameron-Smith, P. Impacts of shifts in phytoplankton community on clouds and climate via the sulfur cycle. *Glob. Biogeochem. Cycles* **32**, 1005–1026 (2018).

45. Bar-On, Y. M., Phillips, R. & Milo, R. The biomass distribution on Earth. *Proc. Natl Acad. Sci. USA* **115**, 6506–6511 (2018).

46. Alsos, I. G. et al. Sedimentary ancient DNA from Lake Skartjørna, Svalbard: assessing the resilience of Arctic flora to Holocene climate change. *Holocene* **26**, 627–642 (2016).

47. Kock, K. H. & Everson, I. Shedding new light on the life cycle of mackerel icefish in the Southern Ocean. *J. Fish Biol.* **63**, 1–21 (2003).

48. Ducklow, H. W. et al. Marine pelagic ecosystems: the West Antarctic Peninsula. *Phil. Trans. R. Soc. B* **362**, 67–94 (2007).

49. Massolo, S., Messa, R., Rivaro, P. & Leardi, R. Annual and spatial variations of chemical and physical properties in the Ross Sea surface waters (Antarctica). *Cont. Shelf Res.* **29**, 2333–2344 (2009).

50. Rivaro, P. & Ianni, C. Biogeochemistry of the Ross Sea and its ecosystem implication. *Deep Sea Res. II* **219**, 105449 (2025).

51. Panasiuk, A., Wawrzynek-Borejko, J., Musiał, A. & Korczak-Abshire, M. *Pygoscelis* penguin diets on King George Island, South Shetland Islands, with a special focus on the krill *Euphausia superba*. *Antarct. Sci.* **32**, 21–28 (2020).

52. Haberman, K. L., Ross, R. M. & Quetin, L. B. Diet of the Antarctic krill (*Euphausia superba* Dana): II. Selective grazing in mixed phytoplankton assemblages. *J. Exp. Mar. Biol. Ecol.* **283**, 97–113 (2003).

53. Clucas, G. V. et al. A reversal of fortunes: climate change 'winners' and 'losers' in Antarctic Peninsula penguins. *Sci. Rep.* **4**, 5024 (2014).

54. Buchwald, S. Z., Herzschuh, U., Nürnberg, D., Harms, L. & Stoof-Leichsenring, K. R. Plankton community changes during the last 124 000 years in the subarctic Bering Sea derived from sedimentary ancient DNA. *ISME J.* **18**, wrad006 (2024).

55. Fan, G. et al. Southern Ocean carbon export efficiency in relation to temperature and primary productivity. *Sci. Rep.* **10**, 13494 (2020).

56. Fetterer, F., Knowles, K., Meier, W., Savoie, M. & Windnagel, A. K. *Sea Ice Index, Version 2* (National Snow and Ice Data Center, 2016); https://doi.org/10.7265/N5736NV7

57. *Antarctic Digital Database Version 7.0* (Scientific Committee on Antarctic Research, 2020); https://www.add.scar.org/

58. *Quantarctica (Version 3.2)* (Norwegian Polar Institute, 2021); https://quantarctica.npolar.no

59. Monnin, E. et al. Atmospheric CO_2 concentrations over the last glacial termination. *Science* **291**, 112–114 (2001).

[1]Polar Terrestrial Environmental Systems, Alfred-Wegener-Institute Helmholtz Centre for Polar and Marine Research, Potsdam, Germany. [2]Institute of Environmental Science and Geography, University of Potsdam, Potsdam, Germany. [3]Institute of Biology and Biochemistry, University of Potsdam, Potsdam, Germany. [4]Marine Geology, Alfred-Wegener-Institute Helmholtz Centre for Polar and Marine Research, Bremerhaven, Germany. [5]Department of Geosciences, University of Bremen, Bremen, Germany. [6]MARUM – Center for Marine Environmental Sciences, Bremen, Germany. [7]Institute for Geology, University of Hamburg, Hamburg, Germany. [8]Laboratoire Chrono-environnement, UMR 6249-CNRS, Université Marie et Louis Pasteur, Besançon, France. [9]These authors jointly supervised this work: Ulrike Herzschuh, Kathleen R. Stoof-Leichsenring. ✉e-mail: josefine-friederike.weiss@awi.de; ulrike.herzschuh@awi.de; kathleen.stoof-leichsenring@awi.de

Methods

Sediment core PS97/072-01

During the RV *Polarstern* cruise PS97 to the Drake Passage in 2016, sediment core PS97/072-1 was retrieved with a piston corer from the east Bransfield Strait (northern Antarctic Peninsula; 62.0065° S, 56.0643° W). The core was recovered from a water depth of 1,992.9 m and the total usable length was 1,012 cm (ref. [60]). The sediment of the core is described as a silty diatomaceous clay and the age model as well as microfossils, total organic carbon, biogenic opal and the biomarker data have been previously published[11].

X-ray fluorescence core scanning

Sediment core PS97/072-01 was scanned using an Avaatech X-ray fluorescence core scanner. Scanning resolution was 1 cm with a detected area of 10 × 12 mm along the core. The elements Fe and Ba were measured with 10 kV and a 150 µA No-filter (10 s) and with 50 kV and a 1,000 µA Cu-filter (20 s), respectively.

The obtained results are estimations of relative element concentrations, provided in total counts per second, and are considered semi-quantitative. These estimations were derived by evaluating the intensities of the detected peak areas, as described by ref. [61]. The Ba and Fe count data were normalized based on the Ba/Fe element ratio, a method established by ref. [12] (Supplementary Data 3). Furthermore, the ratio was subjected to a smoothing process to enhance its consistency.

Extraction of sedaDNA

Halved sediment cores were subsampled under clean conditions in the climate chamber at German Research Centre for Geosciences devoid of any molecular biological work (Supplementary Information). The sediment core was subsampled for 63 samples. DNA extraction of sediment samples (5–10 g wet weight) was accomplished using the DNeasy PowerMax Soil Kit (QIAGEN). Samples were extracted in seven batches of nine samples and one extraction blank, which was included for generally monitoring the cleanliness of the extraction procedure.

DNA extracts were purified and concentrated with the GeneJET PCR Purification Kit (Thermo Fisher Scientific). DNA concentrations were measured with a Qubit 4.0 fluorometer using the BR Assay Kit (Invitrogen) and adjusted to a final concentration of 3 ng µl^{-1}.

Shotgun metagenomics

For the metagenomic approach, 34 samples (about every ~250 years) and 10 blanks were selected (Supplementary Data 1). Associated extraction blanks were included in our six library batches, each containing five or six samples. Additionally, library blanks containing only library chemicals were added to each library batch (Supplementary Data 2). Single-stranded DNA libraries were produced following the protocol of ref. [62] with modifications described in ref. [63]. In short, after the library build, the libraries were quantified using quantitative PCR to calculate the number of amplification cycles for index PCR. Sample libraries were amplified with 11–13 cycles (blank libraries with 11 cycles) using the indexing primers P5 (5′–3′: AAT GAT ACG GCG ACC ACC GAG ATC TAC ACN NNN NNN ACA CTC TTT CCC TAC ACG ACG CTC TT; IDT) and P7 (5′–3′: CAA GCA GAA GAC GGC ATA CGA GAT NNN NNN NGT GAC TGG AGT TCA GAC GTGT; IDT), the AccuPrime Pfx polymerase (Life Technologies) and 24 µl of each library. Finally, the sample libraries were pooled equimolar, while extraction blanks and library blanks were pooled with 1 µl. The library pool was purified and adjusted to the required volume (10 µl) and molarity (20 nM) by using the MinElute PCR Purification Kit (QIAGEN). Sequencing was conducted on a NextSeq 2000 (Illumina) device using the NextSeq 2000 P3 Reagents (200 cycles).

Bioinformatic processing

Raw sequencing data for samples and blanks were quality checked with FastQC (version 0.11.9), and adaptor trimmed and merged using Fastp (version 0.20.1). Results of the quality check of the sequencing data are given in Supplementary Data 1. The taxonomic classification of passed reads was conducted with Kraken2 (ref. [64]) at a confidence threshold of 0.8 against the non-redundant nucleotide database (built with Kraken2 in April 2021).

The Kraken2 report files were then processed with a Python script[65] to add the full taxonomic lineage to each TaxID. Further analyses were performed in RStudio (v.1.2.5001; R v.4.0.3). Using the dplyr package (v.0.7.8.), the metadata, the TaxID table and the Kraken report were merged using the left_join function[66].

Ancient damage pattern analysis

The selection of key taxa for ancient damage patterns includes *Phaeocystis antarctica* (haptophyte), *Chaetoceros simplex* (diatom), *Methylophaga nitratireducenticrescens* (bacteria) and *Pseudochaenichthys georgianus* (crocodile ice fish). Prior to the analysis of damage patterns, we grouped samples into five groups of adjacent age: group 1 (0.01–7.8 kyr old), group 2 (8.2–9.7 kyr old), group 3 (10.5–11.4 kyr old), group 4 (11.9–12.6 kyr old) and group 5 (12.8–13.9 kyr old). We then summed up the raw sequencing files with the cat command and repeated the bioinformatic processing (quality filtering, merging and classification with Kraken2) on the groups. The Kraken2 output files were used to extract taxon-specific reads, which were subsequently used for mapping reads against selected reference sequences in mapDamage2.0 (v. 2.0.8)[67] for the estimation of misincorporation rates due to post-mortem damage. mapDamage2.0 was run with the options rescale (estimates the damage probability at each position in the read from the base quality scores) and single-stranded (because a single-stranded library protocol was used and deamination rates in single-stranded regions are higher). The frequency of post-mortem C to T changes are presented in the Supplementary Information (section 'Post-mortem damage patterns').

Statistics

The following analyses were all performed using RStudio (v.1.2.5001; R v.4.0.3). The graphics were exported from R as vector graphics (for example, PDF) to be further enhanced with the graphics program Inkscape (Inkscape 1.1.2 (b8e25be8, 2022-02-05)). The map was created using QGIS and the Quantarctica package (v3.2; Norwegian Polar Institute)[58].

The data from elemental scanning were normalized using the package compositions[68]. For the Ba/Fe ratio, we used the additive logarithmic ratio transformation function (alr). To fit the Ba/Fe ratio and biomarker data to the shotgun sequencing age data points, we used the linear interpolation function (=FORECAST) in Excel (v. 16.74) and the interpolated data points later on for further analysis.

The EPICA Dome C data derived from refs. [28,59] were transformed using a translator of 650 for the secondary axis to plot both within one graphic with a 0.99 confidence level and a span of 0.1.

For the primary producer community, we only included taxa with a relative abundance greater than 1% per sample and a minimum taxonomic classification to genus level. We followed a script[69] for resampling to normalize this dataset[26]. For the higher trophic levels, we included only Antarctic taxa without a minimum relative abundance threshold. The relative abundance of the methylotrophic bacteria (Methylophilaceae, Methylobacteriaceae, Hyphomicrobiaceae, Beijerinckiaceae, Methylococcaceae and *Methylophaga* (or their relatives)) was calculated against the primary producer abundance.

The overall contamination of the blanks was minor (Supplementary Data 2). One species that was identified as methylotrophic prokaryote was represented in one blank with one read count (*Methylobacterium durans*). *M. durans* was therefore excluded from the analysis (nine reads in two samples). Altogether, methylotrophic bacteria had a read count of 11,057 without *M. durans*.

The community composition over time is depicted in a stratigraphic diagram with the information of relative abundance using the

R packages tidyverse[63], tidypaleo[70] and ggplot2 (ref. [71]). The arrangement of the plots was done using the cowplot package[72], followed by Inkscape to align them. The ecosystem drawings were done using Inkscape (Inkscape 1.1.2 (b8e25be8, 2022-02-05)).

To analyse the community and ecological turnover over time, we performed a latent Dirichlet allocation and added a change-point model (Supplementary Information). For further multivariate statistical analysis of the environmental and palaeogenetic data we applied an SEM. First we interpolated the data at consistent 300-year intervals using the rioja package interp.dataset function[73] and log transformed the phytoplankton relative abundance and temperature data. We focused on the most abundant phytoplankton taxa, including *Chaetoceros*, *Fragilariopsis* and *Phaeocystis*. To uncover carbon cycle dynamics, we used linear mixed-effects models with environmental factors and phytoplankton as fixed effects and time as a random effect. We fitted these linear mixed-effects models with the lme function from the nlme package[74], examining the influence of temporal fluctuations. The model also aided the identification of alternative paths leading to a more exploratory approach due to the absence of prior hypotheses for these paths.

Subsequently, we implemented a piecewise SEM using the piecewiseSEM R package[75] to comprehensively understand the direct and indirect effects of these variables on the carbon cycle. Structural equation modelling is a statistical method that allows for modelling complex relationships between multiple variables simultaneously. It captures both direct and indirect effects between variables, helping to uncover how they influence each other in a system. A piecewise SEM is a specialized form that divides the modelling process into separate segments or 'pieces'. This approach is particularly useful when different relationships or stages of the model are best represented in distinct parts, rather than a single integrated model. By breaking down the relationships into manageable sections, the piecewise SEM enables clearer interpretation and better handling of varying dynamics between the variables. In the piecewise SEM, the Fisher's *C*-test evaluates the goodness-of-fit of the model, where a large *P* value (>0.05) indicates that the model fits the data well, meaning there are no significant deviations. The AIC is used for model comparison, with lower AIC values indicating a better trade-off between model fit and complexity. The chi-squared statistic also assesses model fit, where a small χ^2 value and a large *P* value suggest that the model adequately represents the data. Conversely, the *P* values of standardized coefficients in the model indicate the significance of each predictor, with smaller *P* values (<0.05) suggesting that the corresponding variable has a statistically significant effect on the outcome. Thus, while large *P* values are desirable for assessing overall model fit, smaller *P* values are preferred for evaluating the significance of individual predictors[75].

Model selection based on these factors confirmed that our model, considering specific environmental factors and phytoplankton abundance, provided the best prediction of the carbon cycle dynamics (Supplementary Data 4).

Calculation of cumulative CO_2 drawdown and conversion to atmospheric CO_2 change

The projection of the impact of NPP on global CO_2 concentrations was performed using R and the R package pracma[76]. The estimates for CO_2 drawdown were calculated using a formula that includes known estimates for the NPP for *Phaeocystis*, *Fragilariopsis* and *Chaetoceros*, the sea-ice extent and different atmospheric–oceanic flux estimates. Accumulating our calculations for the pre-ACR, ACR and post-ACR resulted in the cumulative CO_2 drawdown (CCD) estimates for the three different time periods. These estimates were then statistically tested against the observed CO_2 values using a paired *t*-test. Considering varying flux rates (CO_2 ocean–atmosphere exchange) and varying NPP values allowed us to evaluate the uncertainties of our approach.

$$CCD = (NPP\{min, mean, max\} \times 0.3) \times SSIA$$
$$\times t \times 10^{-15} \times Flux\{0.3, 0.5, 0.7\} \times 0.128$$

(1)

Here, NPP {min, mean, max} represents the minimum, mean and maximum values of NPP ($gC\,m^{-2}\,yr^{-1}$) of primary producers, specifically for *Phaeocystis antarctica*, *Fragilariopsis* and *Chaetoceros*, based on literature data for the Ross Sea and modern Western Antarctic Peninsula. To create the most accurate outcome, we reduced NPP measurements in modern Southern Ocean environments to only 30% as suggested by ref. [77] due to a lower CO_2 partial pressure in the atmosphere. The seasonal sea-ice extent area (SSIA), which directly influences the area of primary production, derived from ref. [8]. The variable *t* represents the time period over which the calculations were made (1,800 years for the ACR period in our study). The flux values (0.3, 0.5 and 0.7) are used to account for variations in the flux between the atmosphere and the ocean, reflecting different assumptions about the CO_2 exchange dynamics[77]. The factor 0.128 is a conversion constant that translates the resulting $GtCO_2$ into a change in atmospheric CO_2 concentration (ppm). This factor is derived from the mass of the Earth's atmosphere and the molecular weight of CO_2, where 1 $GtCO_2$ corresponds to a change of 0.128 ppm CO_2 in atmospheric concentration.

By multiplying these components, the equation yields an estimate of the total CO_2 drawdown in gigatonnes, which is then converted to parts per million. This provides an estimate of the cumulative CO_2 drawdown in atmospheric concentration over the specified time period, allowing us to evaluate the impact of primary producers like *Phaeocystis*, *Fragilariopsis* and *Chaetoceros* on atmospheric CO_2 during the ACR. These results help to assess the role of biological processes in CO_2 drawdown during this critical climatic interval.

Data availability
The raw metagenomic sequencing data are available on the European Nucleotide Archive under the accession number PRJEB74305. Source data are provided with this paper.

Code availability
The code is available via Zenodo at https://doi.org/10.5281/zenodo.15705957 (ref. [78]).

References
60. Lamy, F. & Müller, J. Documentation of sediment core PS97/072-1. *Alfred Wegener Institute - Polarstern Core Repository, PANGAEA* https://doi.org/10.1594/PANGAEA.864405 (2016).
61. Richter, T. O. et al. The Avaatech XRF core scanner: technical description and applications to NE Atlantic sediments. *Geol. Soc. Lond. Spec. Publ.* **267**, 39–50 (2007).
62. Gansauge, M. T. et al. Single-stranded DNA library preparation from highly degraded DNA using T4 DNA ligase. *Nucleic Acids Res.* **45**, e79 (2017).
63. Schulte, L. et al. Hybridization capture of larch (*Larix* Mill.) chloroplast genomes from sedimentary ancient DNA reveals past changes of Siberian forest. *Mol. Ecol. Resour.* **21**, 801–815 (2021).
64. Wood, D. E., Lu, J. & Langmead, B. Improved metagenomic analysis with Kraken 2. *Genome Biol.* **20**, 257 (2019).
65. Dinkel, V. Download taxonomic lineage. *GitHub* https://github.com/v-dinkel/downloadTaxonomicLineage (2023).
66. Wickham, H. et al. Welcome to the tidyverse. *J. Open Source Softw.* **4**, 1686 (2019).
67. Jónsson, H., Ginolhac, A., Schubert, M., Johnson, P. L. & Orlando, L. mapDamage2.0: fast approximate Bayesian estimates of ancient DNA damage parameters. *Bioinformatics* **29**, 1682–1684 (2013).
68. van den Boogaart, K. G. & Tolosana-Delgado, R. "compositions": a unified R package to analyze compositional data. *Comput. Geosci.* **34**, 320–338 (2008).

69. Kruse, S. R-rarefaction. *GitHub* https://github.com/StefanKruse/R_Rarefaction (2022).

70. Dunnington, D. W., Libera, N., Kurek, J., Spooner, I. S. & Gagnon, G. A. tidypaleo: visualizing paleoenvironmental archives using ggplot2. *J. Stat. Softw.* **101**, 1–20 (2022).

71. Wickham, H. et al. ggplot2: Create Elegant Data Visualisations Using the Grammar of Graphics. R package version 2. https://ggplot2.tidyverse.org (2016).

72. Wilke, C. O. cowplot: Streamlined Plot Theme and Plot Annotations for 'ggplot2'. R package version 1.1.0. https://CRAN.R-project.org/package=cowplot (2020).

73. Juggins, S. rioja: Analysis of Quaternary Science Data (version 1.0-7) https://cran.r-project.org/package=rioja (2020).

74. Pinheiro, J., Bates, D., DebRoy, S., Sarkar, D. & R Core Team nlme: Linear and Nonlinear Mixed Effects Models. (version 3.1-168) https://CRAN.R-project.org/package=nlme (2023).

75. Lefcheck, J. S. piecewiseSEM: piecewise structural equation modelling in R for ecology, evolution, and systematics. R Package version 2.3.0.1. *Methods Ecol. Evol.* **7**, 573–579 (2016).

76. Borchers, H. pracma: Practical Numerical Math Functions. R package version 2.4. https://cran.r-project.org/web/packages/pracma/index.html (2023).

77. Arrigo, K. R., van Dijken, G. & Long, M. Coastal Southern Ocean: a strong anthropogenic CO_2 sink. *Geophys. Res. Lett.* **35**, (2008).

78. Weiß, J. F. et al. JoFrieWeiss/Weiss-et-al.-2025-R-script: Carbon drawdown by algal blooms during Antarctic Cold Reversal from sedimentary aDNA (sedaDNA). *Zenodo* https://doi.org/10.5281/zenodo.15705958 (2025).

Author contributions

K.R.S.-L. and U.H. conceived the study. M.-E.V. and J.M. provided sediment core material and data on geochemical proxies and diatom count. A.P. contributed the analysis of bacteria. K.R.S.-L. supervised the laboratory works. J.F.W. performed bioinformatic analyses. J.F.W. and J.L. performed the statistical data analyses. U.H. and J.F.W. wrote the first draft of the paper, which all authors commented on.

Competing interests

The authors declare no competing interests.

Additional information

Supplementary information The online version contains supplementary material available at https://doi.org/10.1038/s41561-025-01761-w.

Correspondence and requests for materials should be addressed to Josefine Friederike Weiß, Ulrike Herzschuh or Kathleen R. Stoof-Leichsenring.

Peer review information *Nature Geoscience* thanks Ines Barrenechea Angeles, Marco Coolen, Oscar Schofield and the other, anonymous, reviewer(s) for their contribution to the peer review of this work. Primary Handling Editor: James Super, in collaboration with the *Nature Geoscience* team.

Reprints and permissions information is available at www.nature.com/reprints.